SACLANT UNDERSEA RESEARCH CENTRE REPORT

THE OCEAN WAVE DYNAMO:
A SOURCE OF MAGNETIC AMBIENT NOISE

J. Watermann

September 1997

19980522 066

DTIC QUALITY INSPECTED 4

The SACLANT Undersea Research Centre provides the Supreme Allied Commander Atlantic (SACLANT) with scientific and technical assistance under the terms of its NATO charter, which entered into force on 1 February 1963. Without prejudice to this main task — and under the policy direction of SACLANT — the Centre also renders scientific and technical assistance to the individual NATO nations.

NORTH ATLANTIC TREATY ORGANIZATION

The ocean wave dynamo: a source of magnetic ambient noise

Jürgen Watermann

Jan L. Spoelstra
Director

intentionally blank page

The ocean wave dynamo: a source of magnetic ambient noise

Jürgen Watermann

Executive Summary: The local distortion of the geomagnetic field, caused by the magnetic moment of a submarine, is not the sole source of geomagnetic field deviations from an otherwise static and locally uniform structure. The dynamo effect of moving sea water constitutes just one of various natural and anthropogenic sources which contribute to temporal and spatial geomagnetic variations. Magnetometers at fixed positions on the sea bottom may register a degradation of signal resolution caused by magnetic field variations generated by the motion of sea water. A moving submarine may remain within the detection range of a fixed ocean bottom magnetometer between ten and a thousand seconds, depending on size and speed of the submarine and its distance from the sensor. The dynamo effect of sea surface waves can contribute to the magnetic field fluctuations at the lower end of this range. Incidentally, the range of the potentially detectable geomagnetic field distortion caused by submarines, tens to hundreds of metres, coincides with the typical wave lengths of ocean waves. Ocean waves have therefore to be taken into consideration as a source of magnetic ambient noise. The problem exists mainly in shallow water with a depth not exceeding the wavelength of the surface waves. At greater depth, the magnetic field fluctuations from surface waves are attenuated to an extent which renders them negligible at the sea bottom.

Different theoretical approaches have been pursued in order to determine the intensity of the magnetic field perturbation caused by ocean waves, and a number of experiments have been performed in the past, some of which yielded inconsistent results. We have investigated the magnetic effect of sea surface waves in the Tyrrhenian Sea experimentally, using simultaneously recording island-based and ocean bottom magnetometers. Detailed spectral analysis with close inspection of the power ratio and the phase shift between various components of the magnetic field vector, revealed that dual-sensor measurements of the magnetic field of sea surface waves can be performed with sufficient accuracy to reconstruct solely from magnetic field vector observations, the motion of the water mass elements in the surface wave field. By comparison of spectra computed from data segments recorded on different days we can demonstrate that the scaling, i.e. the relation between surface wave frequency and height and the magnetic field amplitude is quantitatively reproducible and consistent with theoretical predictions.

We found that the magnetic field of ocean waves, although detectable, is very weak in Mediterranean waters. Alleged observations of extremely large amplitudes, sometimes reported in the literature, seem to be incorrect. Our own sea-bottom measurements as well as some of the measurements reported in the literature revealed that magnetometers placed in very shallow water are vulnerable to mechanical vibrations caused by the moving sea water. Mechanical oscillations of the sensor of less than 1 arcsec amplitude can produce an apparent magnetic field fluctuation equal to the dynamo field of surface waves several metres high. This phenomenon may have contaminated those data which seem to suggest an excessively large magnetic dynamo field.

We conclude that the magnetic field associated with sea surface waves is an interesting phenomenon which provides for quantitative information on their mean period, height and propagation direction. On the other hand, the magnetic field is sufficiently small, in accordance with theoretical predictions, not to jeopardize the potential of an ocean bottom magnetometer array to detect moving submarines. If we place the submarine detection threshold at 100 pT we will rarely encounter, at least in the Mediterranean sea, magnetic field fluctuations caused by the ocean wave dynamo which exceed this threshold.

The ocean wave dynamo: a source of magnetic ambient noise

Jürgen Watermann

Abstract: The electromagnetic dynamo field of sea surface waves, a consequence of the Lorentz force, has been measured with two simultaneously operating, closely spaced tri-axial magnetometers. Measurements from a magnetometer located in the centre of a small, uninhabited island served to compensate measurements from a near-shore magnetometer for large-scale magnetic pulsations (basically of ionospheric origin), leaving the ocean wave dynamo field, effective close to shore only, as the dominant residual magnetic field. Height and period of waves and swell were recorded with a vertical accelerometer (wave rider buoy) floating nearby on the sea surface. Amplitude and phase relationships between the three vector components of the magnetic field differences yield an ocean wave vector consistent with swell propagating northeastward. The magnetic field data further demonstrate that the water mass motion close to shore was not confined to a vertical plane (as would be the case for freely propagating gravity waves in the open ocean). The motion occurred in a plane inclined at about 40° from the horizontal (roughly twice the inclination of the island flanks).

Ten night-time intervals of three hours each were analysed, and for every interval, the peak power of the surface waves (inferred from the wave rider measurements) was compared with the peak power of the residual horizontal magnetic field (after the background field had been removed). Their ratio yields the height of a hypopthetical magnetometer above the surface of the open sea. Not only are the hypothetical heights computed for the ten different intervals similar, they are also approximately equal to the horizontal distance between the shoreline and the site of the near-shore magnetometer.

Our results suggest that the island-based dual-sensor magnetic field observations yield, within the limits of statistical significance, a reproducible quantitative description of the amplitude and frequency of sea surface waves and swell, and of the mean water mass motion within about one wavelength from shore. Our results further suggest that the surface wave dynamo field is in quantitative agreement with predictions from classical theory. We can not confirm reports in the technical literature about an allegedly excessively intense ocean wave dynamo field.

Contents

1

Introduction

Natural ULF fluctuations of the geomagnetic field derive predominantly from the combined effects of primary electric currents flowing in the upper atmosphere and magnetosphere of the earth, and secondary (induced) currents flowing in the earth's crust and upper mantle. When magnetic field measurements are performed in the sea, on the sea bottom, or at low altitude above the sea surface, they sometimes reveal additional oscillations of very low intensity which are associated with the ocean wave dynamo. Sea water that moves with a velocity $\mathbf{v}$ across the geomagnetic main field, $\mathbf{B}_0$, generates an electric $\mathbf{v} \times \mathbf{B}_0$ or Lorentz field which provides for an electromagnetic dynamo force. The high electrical conductivity of sea water (typically between 3 and 6 Sm^{-1}) permits the dynamo to drive an electric current which according to Ampère's law is associated with a magnetic dynamo field.

The dynamo effect of moving sea water was predicted as early as 1832 [1]. The effect, and in particular its electric component, is relatively easy to detect as far as large-scale bulk motion of sea water is concerned (including tidal currents and regional and global ocean currents), and has indeed been observed for more than 100 years [2]. Successful measurements were made mostly of the electric field but also of the magnetic field [3, 4, 5, 6]. However, the relatively small amplitude of electromagnetic fields induced by ocean waves and swell (their magnetic component, for instance, is five to six orders of magnitude smaller than the geomagnetic field and often an order of magnitude below ionospherically and magnetospherically generated geomagnetic fluctuations in the same frequency range) posed considerable problems to their identification in magnetic field observations.

Fostered by improvements in the robustness and sensitivity of magnetic field sensors and by new developments in sensor concepts, the magnetic effect of ocean waves received considerable scientific attention during the 1960's and 1970's. A quantitative theoretical treatment of the surface-wave associated magnetic field above the sea surface was published by Crews and Futterman [7]. Their work was supplemented by Warburton and Caminiti [8] who calculated the sub-surface magnetic field of sea surface waves. Weaver [9] used a novel approach to calculate the magnetic field of sea surface waves above and below the surface of oceans with infinite and finite depth. Beal and Weaver [10] followed with a calculation of the magnetic effects of internal waves in oceans of infinite and finite depth. Fraser [11] calculated the magnetic field of surface waves propagating in very shallow water. Podney [12] worked out a comprehensive theory of the magnetic field perturbations associated with surface and internal waves in oceans of infinite and finite depth. Russian theoretical work on the subject was summarized in [13].

In the wake of the theoretical work, several attempts were undertaken to measure the magnetic field of ocean waves. A number of successful observations were made with total field sensors (i.e. scalar magnetometers). They possess the advantage of suffering minimally or not at all from rotational noise, i.e., from apparent magnetic fluctuations produced by mechanical oscillations of the sensor when it follows the oscillatory movement of the water mass elements. Maclure *et al.* [14] measured simultaneously

magnetic field variations in deep water with a rubidium vapour magnetometer suspended from a spar buoy, and ocean wave period and amplitude with an accelerometer floating on the surface. Fraser [15, 11] deployed a proton precession magnetometer and an echo sounder at 40 m depth on the sea bottom and showed that under the assumption of a mean wave crest length of some 300 m, power spectra of ocean waves and magnetic field variations were consistent with theoretical predictions. Podney and Sager [16, 17] exploited the high sensitivity of SQUID (Superconducting Quantum Interference Device) magnetometers to measure above shallow water the vertical gradient of the east-west component of magnetic field variations. They observed that the magnetic field gradient fluctuated in concert with surface and internal waves which they recorded with pressure sensors, and current meter and thermistor chains, respectively. Ochadlik [18] analysed simultaneously recorded magnetic and oceanographic data and found his results to be consistent with Weaver's theory. In one of his experiments, a helium vapor magnetometer was mounted on a research tower placed in shallow water, and a pressure transducer was installed on the sea bottom. In the other experiment, a dual- sensor helium vapor magnetometer was towed by a plane flying at low altitude over large- amplitude ocean swell.

Klein *et al.* [19] attempted to measure the magnetic field of sea surface waves with a pair of search coils, one horizontally and the other vertically mounted in a non-magnetic frame. The device was deployed on the sea bottom in various shallow water areas of the Mediterranean Sea. The authors suggest that spectral maxima found between 0.1 and 0.2 Hz were a manifestation of the surface wave dynamo field. However, no oceanographic data were presented (e.g. measurements from a pressure sensor or a wave rider) which could have provided evidence that the power maxima in the magnetic field spectra indeed coincided with maxima in the surface wave spectrum. Also, the authors did not report the bottom depth (a parameter necessary to assess the meaning of the data properly), and they did not discuss the possibility of a mechanical sensor oscillation, synchronous with the water mass oscillation, which can become a problem for vector magnetometer measurements. Estimation of the cross spectrum between the horizontal and the vertical magnetic field could have helped to resolve the problem. Further details about the method are given in Annex A.

Experimental work during the last twenty years by Russian scientists, translated into the English language on behalf of the American Geophysical Union, is evaluated in section 6.

2
Measurements

Between 12 and 28 September 1995, geomagnetic and oceanographic measurements were conducted simultaneously on and near the small, uninhabited island of Formica Grande (370 m long, 230 m wide, located at 43.6° N, 10.9° E, 14 km off the Italian west coast). It is the largest of a group of three rocky islands called Formiche di Grosseto, which are aligned on a northwest-southeast striking rock bank rising abruptly from an otherwise flat and gently sloping sea floor (Fig. 1). The transition from the inclined island flanks to the almost level sea floor occurs about 300 m northeast of the island at 100 m depth and 450 m southwest at 115 m depth. An autonomously operating lighthouse, the only significant civilisation landmark on Formica Grande, is powered by solar energy collected with an array of silicon panels stored in truck batteries. The lighthouse building served as field laboratory and housed our technical equipment, including a small Diesel generator. Apart from the generator, which was operated during daytime hours only, no source of anthropogenic electromagnetic noise exists on the island.

Two tri-axial fluxgate magnetometers (Mag1 and Mag2) were operated on the island at various locations. A surface floater housing a vertical accelerometer ("wave rider") recorded continuously the wave height some 600 m southwest of the island. In this report, the term "wave height" denotes the vertical distance between undisturbed sea level and wave crest, not the vertical distance between trough and crest. Several Ocean Bottom Magnetometers (OBMs) were deployed a few kilometres from the island. Data from two of them (M12 and M18) were used for this study. The measurements from the island-based magnetometers, the OBMs, and the wave rider were recorded digitally at 48.25 Hz, 2 Hz and 2.56 Hz sampling rates, respectively. For the main part of this report, we selected data which were collected at night when the generator was shut off and all instruments were powered by batteries. Daytime observations are referred to in Annex A. We further restrict the study to four nights from the first phase of the campaign when one of the island-based sensors (Mag2) was located in the centre of the island (site M2) and Mag1 at its southeastern tip (site M1), close to shore and 160 m away from Mag2 (Fig. 2). The magnetic fluctuations recorded with Mag2 were used to compensate the recordings from Mag1 for magnetic field variations of ionospheric origin. The compensation is necessary because the amplitude of the magnetic field fluctuations induced by swell was almost always smaller (often by an order of magnitude) than the average amplitude of the magnetic field fluctuations of ionospheric origin at the same frequency. Compensation is possible because the horizontal scale length of the ionospheric fluctuations is several orders of magnitude larger than that of the swell, with the consequence that the spatial gradient of the ionospheric fluctuations is much smaller than that of the swell dynamo magnetic field.

Figure 3 shows a ten-minute interval of the northward and eastward components of the magnetic field fluctuations observed with the island shore magnetometer, Mag1, the magnetic field difference between measurements with Mag1 and Mag2, and the same difference enlarged by a factor of ten. For better visibility, the curves are graphically separated with an increasing offset along the ordinate. Obviously, the magnetic field recorded with Mag2 (island centre) does not completely compensate

the measurements from Mag1. In addition to low frequency variations, more or less regular fluctuations of about 7 s dominate the residual time series. The latter are associated with the dynamo field of swell, as described below.

3

Spectral Analysis

We performed a spectral analysis on ten three-hour time intervals of simultaneous magnetometer and wave rider observations, distributed over four different nights between September 14 and 18, 1995. The selection of intervals was dictated by the intensity of swell and wave activity which needed to be sufficiently high to generate a measurable dynamo field. Prior to the spectral analysis, the magnetometer and the wave rider data were low-pass filtered (with 0.4 and 0.5 Hz cutoff, respectively) and decimated to sampling rates of 1 Hz and 1.28 Hz, respectively.

Power density spectra of surface waves and geomagnetic variations in the north, east and vertical components were estimated in two different ways. Smoothed periodogram estimates were obtained by averaging 167 FFT spectra from 128-point time segments with 50% overlap (following a method proposed by Welch [20]). Prior to the transform, each individual time segment was centred and tapered with a 4-point Blackman-Harris window. Under the assumption that the individual time segments were different realisations of the same stationary stochastic process, the tapered segments can be considered to be virtually independent of each other despite overlapping [21]. The number of equivalent degrees of freedom thus reaches 99% of 2×167, which translates into a 99% confidence interval ranging from -1.6 dB to +1.9 dB around the estimated power at each point of the spectrum.

The maximum entropy (ME) method, on the other hand, was applied to the full-length time series. Instead of using the Burg [22] algorithm (which minimizes the residual sum of squares with respect to the highest coefficient), we employed an algorithm described by Barrodale and Erickson [23] (which minimizes the residual sum of squares with respect to all coefficients but requires more computer time and memory). Various criteria to determine the number of ME coefficients (i.e. the order of the stochastic process) have been proposed in the literature [24, 25, 26, 27]. We chose a different way and recalculated the ME spectra for process orders between 4 and 28 and for various time series lengths. We found that for orders exceeding 15 (magnetic field) and 20 (wave height) the spectra varied little with increasing order. We therefore decided to estimate the ME spectra from 15-order and 20-order process representations, respectively, using a combined forward and backward prediction scheme. For the quantitative analysis, only the Welsh periodogram estimates were used; the ME estimates served solely to confirm, through an independent method, the existence of spectral peaks with their power significantly above the background noise level. It transpired that for all ten events the ME and periodogram estimates were identical within the confidence limits.

Figure 4 shows ME auto spectra of the north and east components of the magnetic field fluctuations from Mag1 (upper panel), Mag2 (centre panel) and of the residual field (the difference, computed in the time domain, between Mag1 and Mag2; lower panel). To be able to assess the significance of the magnetic field residual, we have included in each panel the upper limit of the magnetometer self noise, derived from the technical specifications provided by the manufacturer. Also plotted is the effective surface wave spectrum which was obtained by correcting the measured wave height

spectrum for the wave rider response function and multiplying it with a factor ω_0/ω (ω_0 is a reference frequency which we chose as $2\pi \times 0.14$ Hz, and ω the wave angular frequency). This factor accounts for the frequency-dependent efficiency of the ocean wave dynamo: For a bottom depth $D > \lambda/3$ (λ denotes the wavelength), the surface wave dispersion relation can be approximated by $\omega^2 \approx gk$ (g means the gravity acceleration and k the wave number), so that the magnetic dynamo field scales with the factor $(g/k)^{1/2} = g/\omega$ [12].

The spectra shown in Fig. 4 are very smooth, and the spectral power rises above system noise only below 0.2 Hz. The spectra from the near-shore magnetometer (Mag1) show a minor peak at 0.14 Hz which coincides with the peak of the effective wave spectrum. The difference spectrum straddles the system noise level over virtually the entire frequency band, except around 0.14 Hz where the spectral power exceeds the noise by 15 dB (north component) and 20 dB (east component). If the vector time series from the two magnetometers were not identical, their difference would not vanish. Consequently, the power spectra of the difference time series would exhibit a certain level of signal power in addition to and uncorrelated with the system noise. This is not the case, except for frequencies around 0.14 Hz and also for the lowest frequencies. We therefore conclude that the time series from Mag1 and Mag2 are indeed almost identical, except for a quasi-DC component (which gives rise to the residual power at the low end of the spectrum) and oscillations with a mean period of some seven seconds (which produce the spectral peak at 0.14 Hz). This peak is statistically significant at a confidence level of more than 99.9% (a number obtained from the corresponding periodogram estimates). We suggest that it results from the swell dynamo field. The swell dynamo is effective only at the shore site and negligible in the centre of the island. The dynamo field is therefore not cancelled out in the process of differencing the time series from the two magnetometers. We will return to this point further in our discussion.

Figure 5 displays auto spectra from the same time interval, obtained *via* the smoothed periodogram technique described above. It includes, in principle, the spectral information from the lower panel of Fig. 4. Figure 5 is more comprehensive as it shows the power densities of the magnetic field differences from all three components, north, east and vertical. The latter also exhibits a peak near 0.14 Hz, but the larger residual power at low frequencies indicates a lesser degree of correlation between the two sites in the vertical component. We suggest that this can, at least in part, be attributed to contamination by anthropogenic magnetic noise, possibly from an underwater cable. Sea charts of the relevant area indicate that a cable passes Formica Grande at some 1700 m distance in 120 m depth, running at 10° bearing from north, i.e. almost perpendicular to the line connecting M1 with M2. An electric current in the cable would produce a magnetic perturbation the power of which would be lower in the horizontal than in the vertical magnetic field component by a factor of $(1700/120)^2 \approx 200$ (i.e. -46 dB). A change of the cable current intensity by 10 A would result in a 0.1 nT change of the vertical magnetic field difference between M1 and M2. Consequently, low-frequency stochastic fluctuations of the cable current with some 10 A peak-to-peak amplitude can explain the higher residual power in the vertical magnetic field. While evident in the vertical component (at a level of -40 dB), they would be completely concealed in the horizontal components (where they would reach only -86 dB).

Around 0.14 Hz, the north and east components of the magnetic field reach peaks of some 45 pT/Hz$^{1/2}$ and 65 pT/Hz$^{1/2}$, respectively. The peak value of the vertical component can not be determined with equal accuracy as its power is substantial

higher than the system noise level in the entire frequency band below 0.2 Hz, and it is
not possible to distinguish between what can be attributed to wave excitation and
incoherent background noise. Extrapolation of the noise spectrum into the frequency
band where the peak appears, suggests that the peak is likely to reach 50 and
60 pT/Hz$^{\frac{1}{2}}$.

The wave height spectrum yields a peak amplitude of 1.4 m/Hz$^{\frac{1}{2}}$ at 0.14 Hz. The
dotted line represents the original spectrum, the solid line the spectrum corrected for
the wave rider response function and modified with the ocean wave dynamo
efficiency factor. The increasing power at the low-frequency end of the spectrum
(below 0.07 Hz) is probably an artefact of the instrument. It was observed in all
measurements, irrespective of wave amplitude and frequency. The wave rider uses
double integration of acceleration measurements to obtain the amplitude, and a small
but persistent, slowly varying bias can easily be confused with long-period variations.

4

Water Motion Inference

In this section we present an example of the reconstruction of swell-associated water mass motion close to the island, based on the information obtained from the spectral analysis of magnetic field oscillations. We employed the spectral techniques described above, but modified in order to apply it to a six-hour interval instead of the usual three hours. We thus increase the degrees of freedom to 672 and reduce the width of the 99% confidence intervals to -1.2/+1.3 dB (for the auto and cross power) and $\pm14°$ (for the phase spectrum if the coherency exceeds 0.45). The relevant time interval started on September 14, 1995, at 01:11 UTC and ended at 07:11 UTC. It was selected because it fell into the period of the highest swell encountered during the entire campaign. Before 01:10 UTC, radio transmission from the wave rider buoy suffered from failures, and around 07:15 UTC, the magnetic noise level began to rise due to work on the island which impaired correlation between measurements from the two magnetometers.

Figure 6 shows the swell activity over a ten-hour time interval in the form of moving spectra. The interval starts at 00:00 UTC on September 14, 1995, and includes the six hours used for the analysis. Elapsed time (scaled in minutes) starts at the left edge of the upper row, runs toward its right end, continues on the left edge of the middle row, and so forth. The individual spectra were obtained from smoothed periodogram estimates of 512 original (undecimated) data points (i.e. 200 s of measurements), and the start of each new 200-seconds time segment was advanced by 24 s over the previous one. The spectra thus overlap by 88%. The reference points on the time axis coincide with the begin of the time segments. It is obvious that the spectral composition of the swell remained very stable over almost the entire ten-hour interval. The dark vertical bar in the upper row marks the radio transmission failure mentioned above.

A stack of various spectral parameters from the magnetic field difference between sites M1 and M2 is compiled in Fig. 7. The upper panel shows the power spectra of the north, east and vertical differences. This panel is similar to Fig. 5 except that it covers six hours of data. The north, east and vertical components of the magnetic field difference peak at 45 $pT/Hz^{1/2}$, 63 $pT/Hz^{1/2}$ and 57 $pT/Hz^{1/2}$, respectively. The next lower panel shows the cross power of the north/east and east/vertical magnetic field differences, together with the instrument noise level. The cross power is almost everywhere lower than the noise except for the remarkable peak around 0.14 Hz.

The information from the two top panels is combined in the third panel to yield the spectral coherency. The larger residual noise in the vertical component results in a lower coherency between the east and vertical components than between north and east components. Only the very low frequencies, which may be dominated by man-made noise, indicate a higher degree of coherency between the east and vertical components of the magnetic field difference. This is consistent with our suggestion that the measurements were affected by electric current fluctuations in an underwater cable. The north/east coherency exceeds 0.5 within the shaded area and reaches a maximum of 0.81, and the east/vertical coherency exceeds 0.45 in its leftmost section

(from the left edge to the blank delimiter line) and reaches a maximum of 0.48. The coherency distribution demonstrates that there is a substantial degree of correlation between the various magnetic field components in the swell frequency band (in particular between magnetic north and east), while the correlation is poor outside this band.

The bottom panel shows the phase shifts between the two pairs of magnetic field differences, north/east and east/vertical. Because of the low coherency, the phase information is highly uncertain outside the shaded area and most certain inside. Within the shaded areas, the north component lags the east component by some 60° and the east component the vertical component by about 75° on the average.

By combining the spectral amplitudes of the magnetic field vector differences with their phase relationships we can estimate the spectral amplitude, spatial orientation, and rotation sense of the magnetic field polarization. Eventually we can infer the mean motion of the water mass elements in the sea surface wave field and the wave propagation vector. In this case, the magnetometers provide more information about the swell than the data from the (non-directional) wave rider can provide.

The numbers for this time interval are virtually identical to those reported above for the first 3 hours, as the ocean wave field remained very stable for the entire six-hour interval. They are: (1) dominant frequency of swell and magnetic field difference, 0.14 Hz; (2) swell peak intensity, 1.4 $m/Hz^{1/2}$; (3) peak intensities of north, east, and vertical magnetic field differences, 45, 63, and 57 $pT/Hz^{1/2}$, respectively; (4) mean phase lag magnetic north versus east, 60° ($=\pi/3$ rad), and east versus vertical, 75° ($=5\pi/12$ rad). From the swell frequency of 0.14 Hz we infer a wavelength of 75 m using the approximate dispersion relation $\omega^2 \approx gk$. The electrical conductivity of the sea water was measured with two submerged conductivity meters to be 5.3 Sm^{-1} at 40 m depth and 4.6 Sm^{-1} at 90 m depth. The elements of the geomagnetic main field at Formica were: total field strength $B_0=45\mu T$, inclination $I=60°$, declination $D=0°$.

From the numerical values obtained for the peak power densities and phase differences of the magnetic field components we can construct a magnetic field polarization ellipse, assuming a situation in which the magnetic field oscillates monochromatically in three dimensions, with the amplitudes along the north, east and vertical axes equal to the root of their respective peak power densities. In parametric representation, the ellipse is determined by the three functions $x_M (t)$, $y_M (t)$, and $z_M (t)$, which denote the north, east, and vertical magnetic field components, respectively:

$$x_M (t) = A_X \, sin \, (\omega t + \pi/3) \tag{1a}$$

$$y_M (t) = A_Y \, sin \, (\omega t) \tag{1b}$$

$$z_M (t) = A_Z \, sin \, (\omega t - 5\pi/12) \tag{1c}$$

with $\omega = 2\pi \times 0.14$ Hz, $A_X=45$ pT, $A_Y=63$ pT, and $A_Z=57$ pT.

Following [12], the spectral amplitude (not the spectral power) of the magnetic field fluctuations, $B_W(\omega)$, is linearly related to the sea surface wave amplitude, $W(\omega)$, via the electromagnetic dynamo process established by the water mass oscillating in the geomagnetic field. For an observation point at a height h above the sea surface, we find the magnitude of the magnetic dynamo field to be

$$B_W(\omega) = \tfrac{1}{2}\,\mu_0\sigma(g/k)^{\frac{1}{2}}\,exp(-kh)\,B_p\,W(\omega) \tag{2}$$

In this equation, μ_0 denotes the vacuum permeability, σ the electrical conductivity of the sea water, and B_p the projection of the geomagnetic main field on the plane in which the water mass elements circulate. In case of a uniform wave field, B_p is the only relevant geomagnetic field component; the geomagnetic field perpendicular to the polarization ellipse plays no role in the dynamo process. The approximate dispersion relation, $\omega^2 \approx gk$, yields $(g/k)^{\frac{1}{2}} = g/\omega$, so that Eq. (2) can be rewritten to read

$$\omega\,B_W(\omega)\,/\,W(\omega) = \tfrac{1}{2}\,\mu_0\sigma\,g\,exp(-\omega^2 h/g)\,B_p \tag{3}$$

For the following discussion, we introduce a scale factor T which depends only on the electrical conductivity of the sea water, the wavelength, the strength of the geomagnetic main field, and the orientation of the motion ellipse, but not on the distance between magnetic field sensor and wave crests. For ocean depths $D > \lambda/3$, T can be approximated with less than 10% error by the expression

$$T = \tfrac{1}{2}\,\mu_0\sigma\,g\,\omega^{-1}\,B_p \tag{4}$$

We assume that the the mean water mass motion is coplanar with the magnetic field oscillation, as is the case in the open ocean. The water mass oscillation can thus be modelled by a parameterized ellipse similar to the one obtained for the magnetic field

$$x_W(t) = \Sigma^{-1}\,T^{-1}\,A_X\,sin\,(\varphi_0 - \omega t + \pi/3) \tag{5a}$$

$$y_W(t) = \Sigma^{-1}\,T^{-1}\,A_Y\,sin\,(\varphi_0 - \omega t) \tag{5b}$$

$$z_W(t) = \Sigma^{-1}\,T^{-1}\,A_Z\,sin\,(\varphi_0 - \omega t - 5\pi/12) \tag{5c}$$

The scale factor Σ depends on the ratio between wavelength and minimum distance between sensor and waves and contains the parameters and their mutual relations necessary to fulfill Eq. (5a,b,c). We leave Σ unspecified for the moment and return to it further below. The arbitrary phase factor, φ_0, has been added to indicate that we do not need to know the phase relationship between water particle motion and magnetic field oscillation. The actual phase lag is irrelevant for our objective, which is the construction of a mean, time-averaged polarization ellipse; only the relative phase shifts between the three vector components are significant. The sign of the angular frequency, ω, is reversed because the vectors of the polarization ellipses of magnetic field variation and water motion share the same plane but circulate in the opposite direction. The water motion in a wave propagating in eastern direction is right-hand polarized with respect to north while the associated magnetic field variation is left-hand polarized, and *vice versa*. Consequently, the polarization sense of the magnetic field yields an estimate of the wave propagation direction (i.e. the orientation of its k-vector). Note that our ellipse is not confined to a vertical plane, as is the case for freely propagating waves in an unbound ocean.

Figure 8 shows the projection of the mean water motion ellipse on the horizontal plane, positioned below a map of Formica Grande (taken from Fig. 2). North points toward the top and east toward the right. The vertical component of the water motion is represented by different shades of gray, darkest tone means point of lowest, lightest tone means point of highest displacement of the water mass elements. The polarization of the water motion is marked by small curved arrows. Note that island and ellipse are not drawn to scale. The ellipse semi-axes are of the same order of

magnitude as the mean wave amplitude, that is of the order of 1 metre. A more precise scaling is not possible because the amplitude of the water mass displacement close to shore differs from that measured in open water.

The direction from the Strait of Bonifacio (located between Corsica and Sardinia) to the Formiche islands is indicated in Fig. 8 by an arrow across the ellipse. It nearly coincides with the orientation of the major axis of the ellipse projection. Orientation of the major ellipse axis and polarization of the water motion suggest that the surface wave vector, **k**, was pointing approximately northeastward, nearly aligned with the arrow. This is in agreement with long-term observations of ship operators which indicate that swell encountered in the Formiche area very often originates in the Strait of Bonifacio.

The inclination of the ellipse is qualitatively in agreement with the expected water motion. The inclined island flanks allow the rising water to move toward the island centre and force the sinking water to move away from the island centre. For waves not propagating perpendicular to the island flanks, the originally circular motion, which was confined to a vertical plane, is converted into a motion in a plane inclined in the same sense as the island flank. In the case of Formica Grande, the flank gradient at the southeastern edge of the island is mainly south-north oriented. The topography thus forces the water to deviate from the original, southwest-northeast oriented motion in a vertical plane, and to assume an additional north-south motion up and down the island flank, which is approximately in phase with the vertical motion but not with the original horizontal motion. We conclude that the three-dimensional orientation of the ellipse represents qualitatively the true motion of the water mass elements on the island flank. Note that only the water motion very close to the island, within about one wavelength, contributes efficiently to the observed magnetic field oscillation. The discussion further below makes clear that the scale factor Σ becomes very small for distances exceeding one wavelength.

In the case of a uniform surface wave field, the magnetic field polarization ellipse above the sea surface degenerates into a circle. Although the condition of wave field uniformity is certainly violated through the presence of the obstacle Formica Grande, we use it as a first approximation in our description of the water motion. The polarization ellipse is indeed almost circular, the major and minor axes of the fully three-dimensional magnetic field polarization ellipse, for instance, are found to be 64 pT and 61 pT, respectively. In order to facilitate quantitative comparison with theory, we approximate the polarization ellipse by a circle of the same area (which has a radius of 62 pT), and assume a circular water motion with an amplitude equivalent to the wave peak power observed away from the island, i.e. 1.4 m. The intensity of the geomagnetic main field in the plane of the polarization ellipse, B_p, amounts to 22.4 μT.

With these simplifications, we determine a factor S, which is equivalent to Σ in the sense that S relates the height, h, of a hypothetical observation point above the surface of the open sea to the magnitude of the observed dynamo field while Σ does the same but for the horizontal distance, d, between the shoreline and the magnetometer. Following Podney, S can be expressed as

$$S = exp(-kh) \tag{6}$$

In this study, we term h the "equivalent sensor height". Essentially, the parameter h, computed from Eq. (3), tells us how far a magnetic field sensor should have been

placed above the surface of an open ocean in order to observe a circularly polarized magnetic field oscillation confined to a vertical plane and with the same amplitude as was observed at the M1 site (under the condition that the same swell amplitude and frequency prevailed). The numbers for the parameters needed to evaluate Eq. (3), ω, $B_w(\omega)$, $W(\omega)$ and σ were measured, and B_P was derived from the inclination of the polarization plane. We obtain 41 m for the parameter h. Incidentally, this is also roughly the length of the shortest line-of-sight between M1 and the shore where the swell hit the island (approximately southwest of M1; in Fig. 8, it is the point where the arrowhead almost touches the island contour). Mag1 was much closer to the shore at the northwestern side of M1, but at that side the sea was protected by the island, and the waves were not high enough to generate a measurable magnetic dynamo field. It is also from clear Eq. (6) that S is reduced by a factor of the order of 500 if h is replaced by $h+\lambda$, i.e. if the motion of a water mass element at a point one wavelength away from shore is considered. For this reason, only the water motion close to shore contributes effectively to the observed magnetic field oscillation. For the same reason it was sufficient to place our local reference sensor, Mag2, about two wavelengths inland to ensure that it remained practically unaffected by the ocean wave dynamo.

5

Magnetometer/Shore Distance Scaling

The detailed discussion in the preceding section of one representative sample of ocean wave dynamo field observations revealed that the equivalent sensor height, a parameter which follows from theoretical investigations [12] is of the same magnitude as the distance between the shore and M1. This result is not obvious given the fact that our experimental setup was significantly different to the one assumed by Podney in developing his theory, and that there is no compelling reason to assume that the vertical distance between wave crests and a magnetic field sensor placed above the sea surface can be replaced by a quasi-horizontal distance between shore-based magnetometer and nearest wave crest.

Podney and his predecessors developed their theory for the geometrically simple case of an unbound ocean with a plane, strictly horizontal bottom and perfectly two-dimensional, freely propagating gravity waves in which the water mass motion is confined to a vertical plane containing the wave propagation vector. This is different to our situation in which we consider the water motion close to an island with sloped flanks. To our knowledge, the complex topography of an island has not yet been treated analytically. Examples of various topographic structures have, however, been studied experimentally by Miles and Dosso [28, 29], who employed reduced-size analogue models of various representative topographic features and applied consistent scaling to the physical parameters. A numerical simulation of wave propagation and magnetic field excitation in specific topographic settings may provide an alternative approach to dealing with complex topographies. We are not aware that such simulation studies have been published in the publicly accessible literature.

Miles and Dosso performed measurements of wave-induced magnetic fields on laboratory models of various coastal shapes, shelf profiles, dykes and sea mounts. They found that in very shallow water, and close to topographic ocean bottom irregularities, the magnetic dynamo field of surface waves can deviate substantially from the field observed above a uniform ocean. Among the models they investigated, the sea mount model meets best, though not completely, the conditions prevailing at Formica Grande. The scale model of Miles and Dosso is equivalent to a setting in which a 106 m deep ocean with 4.5 Sm^{-1} electrical conductivity is threaded by a vertical magnetic field of 50 μT intensity. A nonconducting sea mount with flanks of 60° inclination, surmounted by a platform which extends over 200 m horizontally, rising up to 7.6 m below the surface. Surface waves of 0.064 Hz frequency propagate in the ocean and across the sea mount. The magnetic field probe is positioned 24 m above the sea surface. The scale model measurements indicate that at the edge of the sea mount (and continuing toward its centre), the magnetic field amplitude can be reduced by some 50% compared to a reference field measured over a deep ocean with a plane bottom.

It is worth calculating for all ten time intervals (events) which we selected for this study, at which hypothetical height h a magnetic field sensor should have been placed if we assumed that the data recorded with Mag1 stem from measurements made above the surface of an open sea with a uniform wave field. We applied the analysis method

described above and computed the equivalent sensor height as explained before. The result is shown in Fig. 9 where h_i (i=1,..,10) is plotted against the peak swell amplitude $W_i(\omega_i)$. In all ten events, $B_{w,i}(\omega_i)$ was computed from the magnetometer data, and ω_i and $W_i(\omega_i)$ from the wave rider data. We notice that the numbers for h_i do not differ substantially between the different events, despite the fact that the wave amplitude spanned half a decade. The mean value was found to be $\hat{h}=37.5$ m and the standard deviation $\sigma_h=5.2$ m.

It should be noted that the total number of events is too small to infer a potential dependence of the hypothetical sensor height on the wave amplitude. At a first glance, one might be tempted to state a slight increase of the hypothetical sensor height with increasing wave height. Such is, however, statistically unfounded. The two isolated, large-amplitude events stem with about 15% probability from the same statistical population as the eight small-amplitude events.

Our results thus provide us with a scaling, $d \approx h$, between an equivalent sensor height h, as assumed in Podney's theory, and the actual horizontal sensor distance d from shore. We conclude that Podney's theory (and Eq. (2) and (3), for that matter) remain approximately correct without further modification if only the sensor height h is substituted by the sensor distance d from shore, i.e., from the nearest possible wave crest.

We must emphasize, however, that the scaling $d \approx h$ is only valid for our particular experimental configuration. In a different place, or with the magnetometers located at different sites, the scaling may be different. Once the scaling between h and d has been determined for the chosen magnetometer configuration, one can infer the ocean wave height from the magnetic field observations without the need for direct measurements of the wave height. The method is constrained only by the condition that the wave propagation direction is known as it is needed to determine B_p. As we have seen in the reconstruction of the water mass motion, it is possible, under the condition of favourably low magnetic ambient noise, to infer the wave vector from the magnetic field observations.

6

Evaluation of Russian Research

Several Russian authors reported observations of the magnetic field associated with sea surface waves and swell [30, 31, 32, 33, 34, 35]. Their measurements were made with magnetometers placed on or buried in the sea bottom in very shallow water (between 3 m and 30 m depth). Some of the papers report amplitudes of the magnetic field variations significantly in excess of those expected from classical theory, in some cases by several orders of magnitude [30, 31, 33]. On the other hand, Rutenko [34] reports magnetic field amplitudes lower than theoretically expected. If the extremely large magnetic field variations cited above would really represent the ocean wave dynamo field, the presence of waves or swell with amplitudes of one metre only could have a devastating effect on the capabilities of a sea-bottom magnetometer array to detect moving submarines.

To give just one example, Fig. 1 of [33] corresponds to a magnetic dynamo field of 1.3 nT at 26 m depth, in the presence of waves with periods of 6 s and amplitudes between 1 and 1.5 m. This would mean a scale factor of about 1 nT/m. Classical theory (i.e. [12]) gives only about 0.1 nT/m for the same parameter combination. A medium-sized submarine passing at some 200 to 300 m distance from the sensor generates a magnetic field distortion of 1 nT. It is the same signal amplitude as 1 m high waves in very shallow water would generate, according to [32].

Among the very few western publications cited by Russian authors, reference [19] is used by Krotevich et al. [31, 33] as a reference for confirming their opinion. Careful reading of the relevant papers reveals that not only is the interpretation given in [19] highly speculative and not supported by the measurements, but also that a statement in [31, 33], attributed to [19] and considered a key result, claiming that the magnetic field parallel to the wave crests is more intense than the magnetic field perpendicular to them, does not appear in [19]. Krotevich et al. [33] cite an earlier paper [32] supposedly containing a similar statement which also does not appear there. Important data are omitted (pressure variations were reportedly measured by Krotevich et al. [32] but are not displayed in their Fig. 2), or axes labels are missing [30].

We also have reservations concerning the methodology. It is extremely difficult to place magnetometers on the sea bottom of the surf zone (between 3 and 30 m depth, as done by the Russians) in a way which guarantees them to be virtually free of oscillatory motions forced upon them by the pressure gradients associated with the surface waves. Note that we repeatedly detected in our own experiments, mechanical sensor oscillations at some 60 m depth which generated an apparent magnetic field, the amplitude of which significantly exceeded the dynamo field (see Annex A for details). In 1996, for instance, we identified beyond doubt mechanical oscillation of an OBM in 58 m depth which was associated with 1 m high surface waves of 8 s duration, whereas no trace of the waves could be detected at 83 m depth. In fact, Fig. 2c of [33] demonstrates clearly that the spectral distribution of the magnetic field variations was identical to the spectral distribution of the magnetometer tilt variations and significantly different to the spectral distribution of the surface wave pressure variations. At the bottom depth valid for their experiment (3 to 5 m), the water particle

motion in a surface wave of 10 m length is attenuated by a factor of the order of 2 while a factor of more than 10 would be needed to explain the shape of their spectra with the dynamo effect. This is, in our opinion, an indicator that sensor motions were measured and not the dynamo field.

In conclusion, it is our firm conviction that Russian reports on measurements of extremely large amplitudes of the dynamo field of sea surface waves are of questionable veracity and should not be considered a valid argument against the use of magnetometers for detecting moving submarines.

7

Conclusion

We have demonstrated that the magnetic dynamo field of ocean waves can be measured reasonably accurately with a dual-magnetometer system in which one sensor, located inland, compensates the measurements from a second sensor, placed close to shore, for large-scale magnetic field variations (predominantly of ionospheric origin). The residual oscillations (i.e. the vector time series representing the magnetic field difference between the two sites) can be used to infer the water mass motion associated with surface waves and swell. Measurements of the magnetic field fluctuations yield an approximate wave vector (i.e. the wave length and the propagation direction of the swell).

However, magnetic field measurements on an island are not yet deemed suitable to determine the wave height accurately. The complexity of the island topography and the subsequent breakdown of various assumptions made in the theoretical papers (such as the infinite depth approximation, which requires $D>\lambda/3$, the plane bottom topography, and the lack of scattering obstacles like islands), render a quantitative description of the wave height and water mass motion uncertain. Although the scaling between hypothetical sensor altitude, h, and measured distance of the magnetometer from shore, d, namely $d{\approx}h$, appeared to be reproducible in our measurements, it may have been accidental and does not necessarily apply in the general case. Our result is neither supported nor contradicted by published theory. We pose the hypothesis that a reproducible distance scaling (not necessarily an equality), once determined for a particular experimental setup, can be applied to the magnetic field observations from that setup to infer the approximate wave height without the need for direct measurements. Further confirmation of our hypothesis is needed before it can be generalised.

References

[1] Faraday, M. Bakerian Lecture: Experimental researches in electricity - second series, *Philosophical Transactions of the Royal Society London*, **122**, 163-194, 1832.

[2] Longuet-Higgins, M. S. The electrical and magnetic effect of tidal streams, *Monthly Notes of the Royal Astronomical Society*, **5**, 285-307, 1949.

[3] Sanford, T. B. Motionally induced electric and magnetic fields in the sea, *Journal of Geophysical Research*, **76**, 3476-3492, 1971.

[4] Chave, A. D., Filloux, J. H., Luther, D. S., Law, L. K., White, A. Observations of motional electromagnetic fields during EMSLAB, *Journal of Geophysical Research*, **94**, 14153-14166, 1989.

[5] Larsen, J. C. Transport and heat flux of the Florida current at 27°N derived from cross-stream voltages and profiling data: theory and observations, *Philosophical Transactions of the Royal Society London*, **A 338**, 169-236, 1992.

[6] Lilley, F. E. M., Filloux, J. H., Mulhearn, P. J., Ferguson, I. J. Magnetic signals from an ocean eddy, *Journal of Geomagnetism and Geoelectricity*, **45**, 403-422, 1993.

[7] Crews, A., Futterman, J. Geomagnetic micropulsations due to the motion of ocean waves, *Journal of Geophysical Research*, **67**, 299-306, 1962.

[8] Warburton, F., Caminiti, R. The induced magnetic field of sea waves, *Journal of Geophysical Research*, **69**, 4311-4318, 1964.

[9] Weaver, J. T. Magnetic variations associated with ocean waves and swell, *Journal of Geophysical Research*, **70**, 1921-1929, 1965.

[10] Beal, H. T., Weaver, J. T. Calculations of magnetic variations induced by internal ocean waves, *Journal of Geophysical Research*, **75**, 6846-6852, 1970.

[11] Fraser, D. C. The magnetic field of ocean waves, *Geophyical. Journal of the Royal Astronomical Society*, **11**, 507-517, 1966.

[12] Podney, W. Electromagnetic fields generated by ocean waves, *Journal of Geophysical Research*, **80**, 2977-2990, 1975.

[13] Sochel'nikov, V. V. The electromagnetic field of three-dimensional surface ocean waves, *Izvestiya, Earth Physics* (English translation), **21**, 130-133, 1985

[14] Maclure, K. C., Hafer, R. A., Weaver, J. T. Magnetic variations produced by ocean swell, *Nature*, **204**, 1290-1291, 1964.

[15] Fraser, D. C. Magnetic fields of ocean waves, *Nature*, **206**, 605-606, 1965.

[16] Podney, W., Sager, R. Measurements of magnetic gradients from ocean waves, *AIP Conference Proceedings*, **44**, 95-105, 1979a.

[17] Podney, W., Sager, R. Measurement of fluctuating magnetic gradients originating from oceanic internal waves, *Science*, **205**, 1381-1382, 1979b.

[18] Ochadlick, A. R. Jr. Measurements of the magnetic fluctuations associated with ocean swell compared with Weaver s theory, *Journal of Geophysical Research*, **94**, 16237-16242, 1989.

[19] Klein, M., Louvet, P., Morat, P. Measurements of electromagnetic effects generated by swell, *Physics of the Earth and Planetary Interior*, **10**, 49-54, 1975.

[20] Welch, P. D. The Use of Fast Fourier Transform for the Estimation of Power Spectra: A Method Based on Time Averaging Over Short, Modified Periodograms, *IEEE Transactions on Audio and Electroacoustics*, **15**, 70-73, 1967.

[21] Harris, F. R. On the use of windows for harmonic analysis with discrete Fourier transform, *Proceedings IEEE*, **69**, 51-83, 1978.

[22] Burg, J. P. Maximum entropy spectral analysis, Ph.D. Thesis, Stanford University, 1975.

[23] Barrodale, I., Erickson, R. E. Algorithms for least-squares linear prediction and maximum entropy spectral analysis - part I: theory, *Geophysics*, **45**, 420-432, 1980.

[24] Akaike, H. A new look at the statistical model identification, *IEEE Transactions on Automatic Control*, **19**, 716-723, 1974.

[25] Akaike, H.A. Bayesian extension of the minimum AIC procedure of auto-regressive model fitting, *Biometrika*, **66**, 237-242, 1979.

[26] Parzen, E. Some recent advances in time series modelling, *IEEE Transactions on Automatic Control*, **19**, 723-730, 1974.

[27] Schwarz, G. Estimating the dimension of a model, *Annals of Statistics*, **6**, 461-464, 1978.

[28] Miles, T., Dosso, H. W. A laboratory analogue model study of ocean-wave induced magnetic fields for cases of non-uniform depths and sea-land interfaces, *Physics of the Earth and Planetary Interior*, **19**, 12-20, 1979.

[29] Miles, T., Dosso, H. W. An analogue model study of ocean-wave induced magnetic field variations near a coastline, *Journal of Geomagnetism and Geoelectricity*, **32**, 151-154, 1980.

[30] Groskaya, Ye. M., Skrynnikov, R. G., Sokolov, G. V. Magnetic field variations induced by the motion of sea waves in shallow water, *Geomagnetism and Aeronomy* (English translation), **12**, 131-134, 1972.

[31] Krotevich, N. F., Semenov, V. Yu., Fonarev, G. A. Results of experimental observations of the magnetic field from sea waves, *Geomagnetism and Aerononomy* (English translation), **17**, 729-731, 1977.

[32] Krotevich, N. F., Panurovsky, V. N., Rutenko, A. N. Measurement of the magnetic field components of ocean waves, Geomagnetism and Aerononomy (English translation), **22**, 729-730, 1982.

[33] Krotevich, N. F., Panurovsky, V. N., Rutenko, A. N. Measurements of surface wave magnetic field components, Geomagnetism and Aeronomy (English translation), **23**, 719-721, 1983.

[34] Rutenko, A. N. Magnetic field variations induced by storm waves in the shore, *Geomagnetism and Aeronomy* (English translation), **21**, 289-291, 1981.

[35] Rutenko, A. N. In situ investigations of electromagnetic field fluctuations induced by surface and internal waves, *Oceanology* (English translation), **35**, 616-622, 1995.

[36] Carlton, P. N. Ocean swell magnetic field simulation, Oceans '72, IEEE International Conference on Engineering in an Ocean Environment, Newport, 316-319, 1972

Annex A: Mechanical Oscillations of an Ocean Bottom Magnetometer

An Ocean Bottom Magnetometer (OBM) may be subject to mechanical forces exerted by the pressure of moving sea water. In a shallow sea, these forces include horizontal oscillatory motions of the water mass elements which are associated with surface waves and swell and can extend to the sea bottom. For the following discussion we assume a uniform surface wave field, a flat bottom, and no significant bulk current, i.e. conditions which apply to the area and time of our 1995 measurements off Formica Grande di Grosseto. In consequence, the water mass motion is confined to a plane spanned by the wave propagation vector, **k**, and a Nadir-pointing vector, **z**.

Let us assume that a tri-axial magnetometer rests on a flat sea bottom oriented in such a manner that its z-axis, denoted by $z^{(M)}$, points vertically down. This is a reasonable assumption for our measurements as the inclination of our OBMs did not exceed $5°$ for all but one magnetometer in both, the 1995 and 1996 sea trials. The orientation of the x- and y-axes of the magnetometer modules, denoted by $x^{(M)}$ and $y^{(M)}$, respectively, cannot be controlled during deployment but can be measured after the module has settled on the bottom. Suppose that the x-axis forms an angle Δ with geomagnetic north (measured clockwise positive). The north, east and vertical components of the geomagnetic main field are denoted by $x^{(G)}$, $y^{(G)}$ and $z^{(G)}$, respectively.

The unit vectors (identified by bold-face lower case letters) along the magnetometer axes are expressed through unit vectors along the geomagnetic north, east and vertical axes by

$$\mathbf{x}^{(M)} = \mathbf{x}^{(G)} \cos\Delta + \mathbf{y}^{(G)} \sin\Delta \qquad \text{(A.1a)}$$

$$\mathbf{y}^{(M)} = -\mathbf{x}^{(G)} \sin\Delta + \mathbf{y}^{(G)} \cos\Delta \qquad \text{(A.1b)}$$

$$\mathbf{z}^{(M)} = \mathbf{z}^{(G)} \qquad \text{(A.1c)}$$

(see also Fig. A1). When the magnetometer module is at rest in a horizontal position, the vector of the geomagnetic main field, **B**, can be expressed in terms of the magnetometer unit vectors as

$$\mathbf{B} = (\mathbf{x}^{(M)} \cos I \cos\Delta - \mathbf{y}^{(M)} \cos I \sin\Delta + \mathbf{z}^{(M)} \sin I) B \qquad \text{(A.2)}$$

with I denoting the inclination of **B** against the horizontal plane (geomagnetic inclination) and $B=|\mathbf{B}|$ the geomagnetic field strength.

Suppose that the magnetometer performs small harmonic rotational oscillations with angular frequency ω around a horizontal axis aligned with the wave crests ("wave crest axis"). This axis shall form an angle Θ with geomagnetic north. Let $\varepsilon \ll 1$ be the amplitude of the oscillation. The instantaneous orientation of the magnetometer axes at an arbitrary point in time, t, can be written as

$$\mathbf{x}^{(R)}(t) \approx \mathbf{x}^{(M)} - \mathbf{z}^{(M)} \sin(\Theta-\Delta)\, \varepsilon \cos(\omega t) \qquad \text{(A.3a)}$$

$$\mathbf{y}^{(R)}(t) \approx \mathbf{y}^{(M)} + \mathbf{z}^{(M)} \cos(\Theta-\Delta)\, \varepsilon \cos(\omega t) \qquad \text{(A.3b)}$$

$$\mathbf{z}^{(R)}(t) \approx \mathbf{z}^{(M)} + [\mathbf{x}^{(M)} \sin(\Theta-\Delta) - \mathbf{y}^{(M)} \cos(\Theta-\Delta)]\, \varepsilon \cos(\omega t) \qquad \text{(A.3c)}$$

In the following we replace "asymptotically equal" with "equal" with which we make an error of second order in ε. The difference between the axes of the fixed and the oscillating magnetometer reads

$$\delta x(t) = x^{(R)}(t) - x^{(M)} = -z^{(M)} \sin(\Theta-\Delta) \, \varepsilon \, \cos(\omega t) \qquad \text{(A4.a)}$$

$$\delta y(t) = y^{(R)}(t) - y^{(M)} = z^{(M)} \cos(\Theta-\Delta)\varepsilon \, \cos(\omega t) \qquad \text{(A4.b)}$$

$$\delta z(t) = z^{(R)}(t) - z^{(M)} = [x^{(M)} \sin(\Theta-\Delta) - y^{(M)} \cos(\Theta-\Delta)] \, \varepsilon \, \cos(\omega t) \qquad \text{(A4.c)}$$

As a consequence of the oscillation, we observe an apparent variation of the magnetic field components along the magnetometer axes of the magnitude

$$b_x(t) = x^{(R)}(t) \cdot \mathbf{B} - x^{(M)} \cdot \mathbf{B} = \delta x(t) \cdot \mathbf{B} = -\sin I \, \sin(\Theta-\Delta) \, B \, \varepsilon \, \cos(\omega t) \quad \text{(A.5a)}$$

$$b_y(t) = y^{(R)}(t) \cdot \mathbf{B} - y^{(M)} \cdot \mathbf{B} = \delta y(t) \cdot \mathbf{B} = \sin I \, \cos(\Theta-\Delta) \, B \, \varepsilon \, \cos(\omega t) \quad \text{(A.5b)}$$

$$b_z(t) = z^{(R)}(t) \cdot \mathbf{B} - z^{(M)} \cdot \mathbf{B} = \delta z(t) \cdot \mathbf{B} = \cos I \, \sin\Theta \, B \, \varepsilon \, \cos(\omega t) \quad \text{(A.5c)}$$

For the Formiche di Grosseto area ($B=45\mu\text{T}$, $I=60°$), we find in the worst case, i.e. $(\Theta-\Delta)=90°$, an apparent magnetic field variation along the magnetometer x-axis of about 0.2 nT/arcsec. In other words, the magnetic dynamo field we observed during the highest sea state encountered in our trial, is equivalent to rotational oscillations of the magnetometer of less than 0.5 arcsec.

The following relations between the three vector components of the apparent magnetic field variations are obtained from Eq. (A.5a,b,c).

$$b_x(t) \, / \, b_z(t) = -\tan I \, \sin(\Theta-\Delta) \, / \, \sin\Theta = -\tan I \, \cos\Delta \, (1-\tan\Delta \, \cot\Theta) \quad \text{(A.6a)}$$

$$b_y(t) \, / \, b_z(t) = \tan I \, \cos(\Theta-\Delta) \, / \, \sin\Theta = \tan I \, \sin\Delta \, (1 + \cot\Delta \, \cot\Theta) \quad \text{(A.6b)}$$

$$b_x(t) \, / \, b_y(t) = -\tan(\Theta-\Delta) \qquad \text{(A.6c)}$$

We note that these ratios, which hold for all combinations of I, Θ and Δ except for obvious singularities in I, Θ, and $(\Theta-\Delta)$, are independent of (ωt). We further note that only phase shifts of $0°$ or $\pm 180°$ can occur between any two of the magnetic field components; phase shifts of $\pm 90°$ are not possible. On the other hand, the phase lag between horizontal and vertical components of the ocean wave dynamo field is $\pm 90°$ in the ideal case of freely propagating gravity waves [17].

In consequence, if a phase shift of $0°$ or $\pm 180°$ is observed between the vertical and the horizontal magnetic field oscillation, we must assume mechanical sensor oscillations, while a phase shift close to $\pm 90°$ suggests magnetic field variations associated with the ocean wave dynamo.

In order to illustrate our point we present in Fig. A2 auto and cross spectra and squared coherences from the OBMs M12 and M18 which resided on the sea bottom at 59 m and 104 m depth, respectively. As the OBMs were not yet in operation during the time interval discussed in section 4, we use data from a six-hour time interval of the following day, September 15. We usually compute the FFT from time series transformed into the geomagnetic $x^{(G)}$-, $y^{(G)}$-, $z^{(G)}$-system or another predefined reference system, but in this case the time series were left aligned with the original magnetometer orientation, $x^{(M)}$, $y^{(M)}$ and $z^{(M)}$, for reasons discussed below. The auto and cross amplitude spectra of M12 have a broad peak close to but not coinciding with the

dominant swell frequency (measured with the wave rider), and the cross phase spectra show phase shifts of almost exactly $0°$ and $\pm 180°$ with a 99% confidence interval of $\pm 14°$. We consider this strong evidence for OBM M12 to have recorded mechanical sensor oscillations.

The auto and cross spectra from simultaneous measurements from M18 do not show traces of the surface waves, neither mechanical oscillations nor dynamo field effects. This is further confirmed by the squared coherency between any two magnetic field components at the swell frequency. It is high for M12 and close to zero for M18.

It is instructive to test Eq. (A.6) on OBM M12 using the example presented in Fig. A2. Under the assumption that the mechanical sensor oscillations and the magnetic background field are uncorrelated and the power of the apparent oscillations is therefore superposed on the background power, we obtain the numerical values, $b_x=0.85$ nT/Hz$^{\frac{1}{2}}$, $b_y=0.59$ nT/Hz$^{\frac{1}{2}}$ and $b_z=0.64$ nT/Hz$^{\frac{1}{2}}$. Application of Eq. (A.6) renders $\Delta \approx -30°$ and $\Theta \approx -90°$, which means a declination of $-30°$ and an east-west orientation of the module swivel axis. This is consistent with rotations in a north-vertical plane. Such motion must be associated with northward or southward propagating waves. From compass measurements on M12 we know that the declination of its x-axis was actually around $9°$. Considering the uncertainties inherent in our crude method (e.g. the proper estimation of the peak and background power), an error of $39°$, (11% of the full circle), is not too bad. Wind measurements made at the same time on Formica Grande indicate predominantly S and SSE wind which is consistent with approximately northward propagating waves. We thus find satisfactory agreement between the propagation direction inferred from magnetometer oscillations and from wind direction measurements.

Finally we draw attention to the fact that the frequency of the ocean waves measured with the wave rider (i.e. at the sea surface) agrees well with the frequency inferred from the island-based magnetometers whereas the frequency of the mechanical oscillations of the OBMs (equal to the frequency of the water mass oscillation close to the sea bottom) tends to be lower than the surface wave frequency. This is a systematic feature of all of our data, not only those shown in this report. A similar phenomenon can be noted in a conference report by Carlton [36] who showed in his Fig. 3 spectra of pressure and horizontal water velocity measured close to the sea bottom together with the spectrum of magnetic field variations (probably measured above the sea surface). Although he states that the spectra are "quite similar", the magnetic field spectrum is obviously systematically offset (to higher frequencies) from the water pressure and velocity spectra.

The explanation is quite simple. A high-frequency (short wavelength) water motion at the sea surface is more attenuated toward the sea bottom than the motion of longer waves. Consequently, the sea bottom water velocity spectrum is dominated by longer periods than the spectrum of waves on the surface. This is shown in Fig. A3 where we compare the spectrum of the vertical water motion, v_z, measured on the surface by the wave rider, with the spectrum of the horizontal water motion, v_h, computed for the sea bottom at a depth, D, of 59 m. To accomplish this, we used the dispersion relation

$$\omega^2 = g\ k\ \tanh(kD) \tag{A.7}$$

in combination with the ratio

$$v_h\ /\ v_z = \coth(kD) \tag{A.8}$$

of the horizontal to vertical velocity amplitudes of the water mass motion immediately below the surface. We assume a simple velocity profile (e.g., [11])

$$v_h(d) = k\ C\ \cosh(kd)\ /\ \cosh(kD) \tag{A.9}$$

with d denoting the height above the sea bottom and C a constant which depends on wave height, wave frequency and water depth but which is eliminated when computing the ratio $v_h(\text{bottom})/v_z(\text{surface})$.

On the other hand, OBMs do not make point measurements of the magnetic field; they measure an integrated, distance-weighted effect from all water mass motions. It is not obvious whether the dynamo field is dominated by the nearby, low-velocity water motion close to the sea bottom, or by the more distant, high-velocity motion closer to the sea surface. Following [17], we have computed the magnetic dynamo field at the bottom of a 59 m deep sea from the wave height spectrum observed at the sea surface. The result is also included in Fig. A3.

We have included in Fig. A3 the spectra of the apparent horizontal and vertical magnetic field oscillations measured with OBM M12, taken from Fig. A2. Their shape is consistent with both, the magnetic dynamo field and the water motion near the sea bottom. The following conclusions can be drawn.

(1) The spectral shapes of the water motion close to the sea bottom and of the dynamo magnetic field to be expected at the sea bottom, are almost identical. It is therefore not possible to determine from the spectral shape whether the OBM has recorded mechanical oscillations or the magnetic dynamo field.

(2) The spectrum of the measured magnetic field exceeds by 40 dB the spectrum of the computed dynamo field (i.e. the observed magnetic field amplitude is one order of magnitude larger than expected). This evidences, in our opinion, the recording of mechanical oscillations of the OBM rather than an observation of the dynamo field.

The wavelength of the swell was of the order of 80 m in this example (a number obtained from the approximate dispersion relation $\omega^2 \approx gk$), and mechanical sensor oscillations were observed at 59 m depth but not at 104 m depth. In another experiment conducted in 1996, we encountered nearly the same swell wavelength and height (some 80 m and 1.5 m, respectively), and observed mechanical sensor oscillations at 58 m depth but not at 83 m depth. It would therefore appear that in order to avoid contamination of our OBM measurements through mechanical motion of the sensor, we need to place the modules at depths exceeding the length of the longest surface waves expected to be encountered during the sea trial. Alternatively, we need to redesign the mechanics of the modules and ballast in order to withstand stronger pressure gradient forcing.
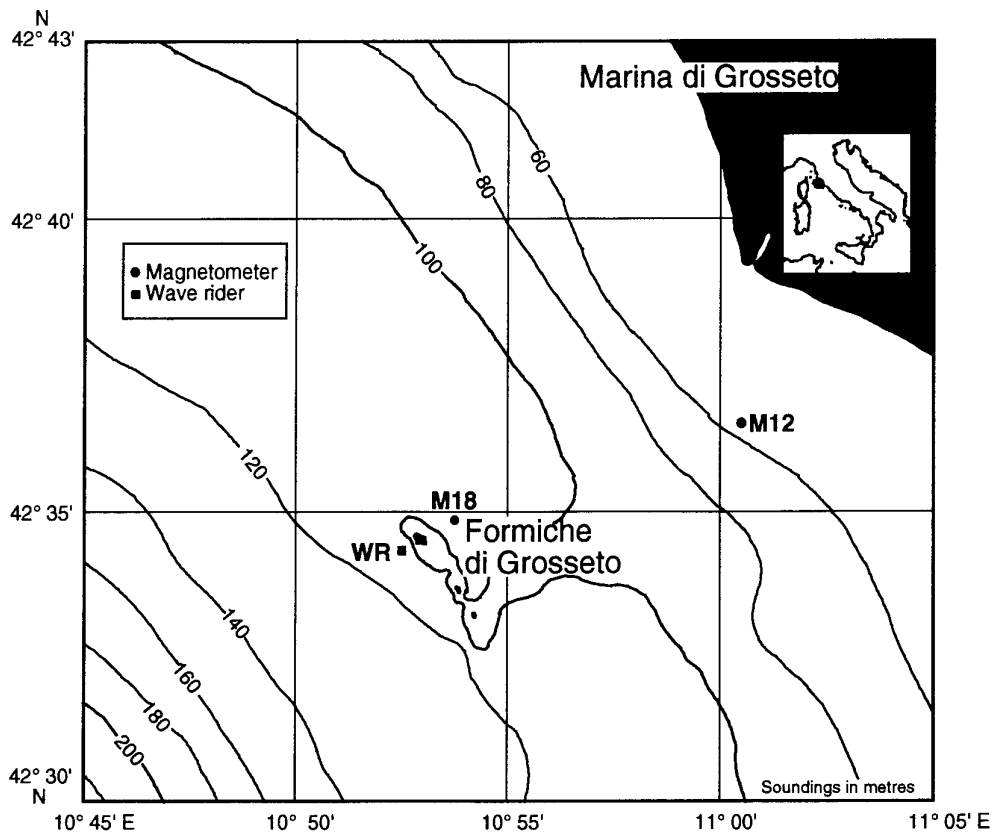
Figure 1 *The Formiche di Grosseto sea area, with part of Tuscany visible in the upper right corner. Inlay map of Italy indicating the location of this area. Bathymetry in metres.*
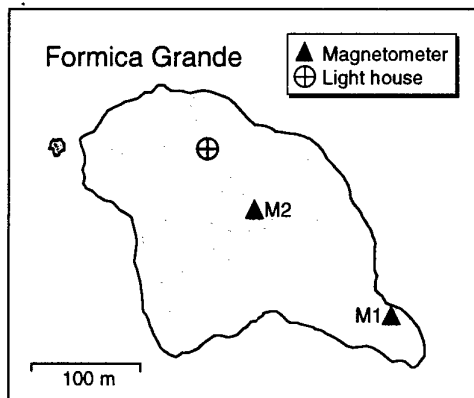

Figure 2 *Formica Grande, the northwestmost island of the Formiche di Grosseto group, with lighthouse and magnetometer sites.*

Magnetic field variations
### Formica Grande di Grosseto, 1995
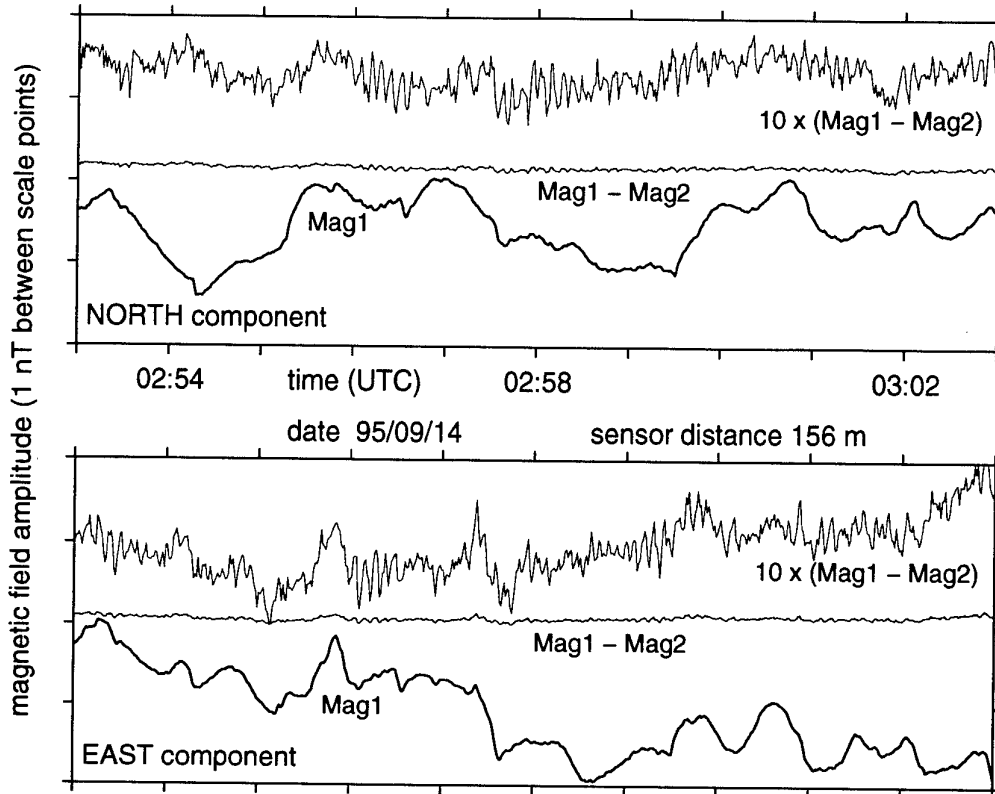
Figure 3 *Ten-minute sample of northward (upper panel) and eastward (lower panel) magnetic field fluctuations observed with Mag1 at site M1 (heavy lines); north and east magnetic field difference between Mag1 and Mag2 (the latter located at site M2), with same amplitude scale as Mag1, and with ten times enlarged scale (thin lines).*

Ocean waves and magnetic field variations

Formica Grande di Grosseto, 95/09/14, 01:11–04:11 UTC
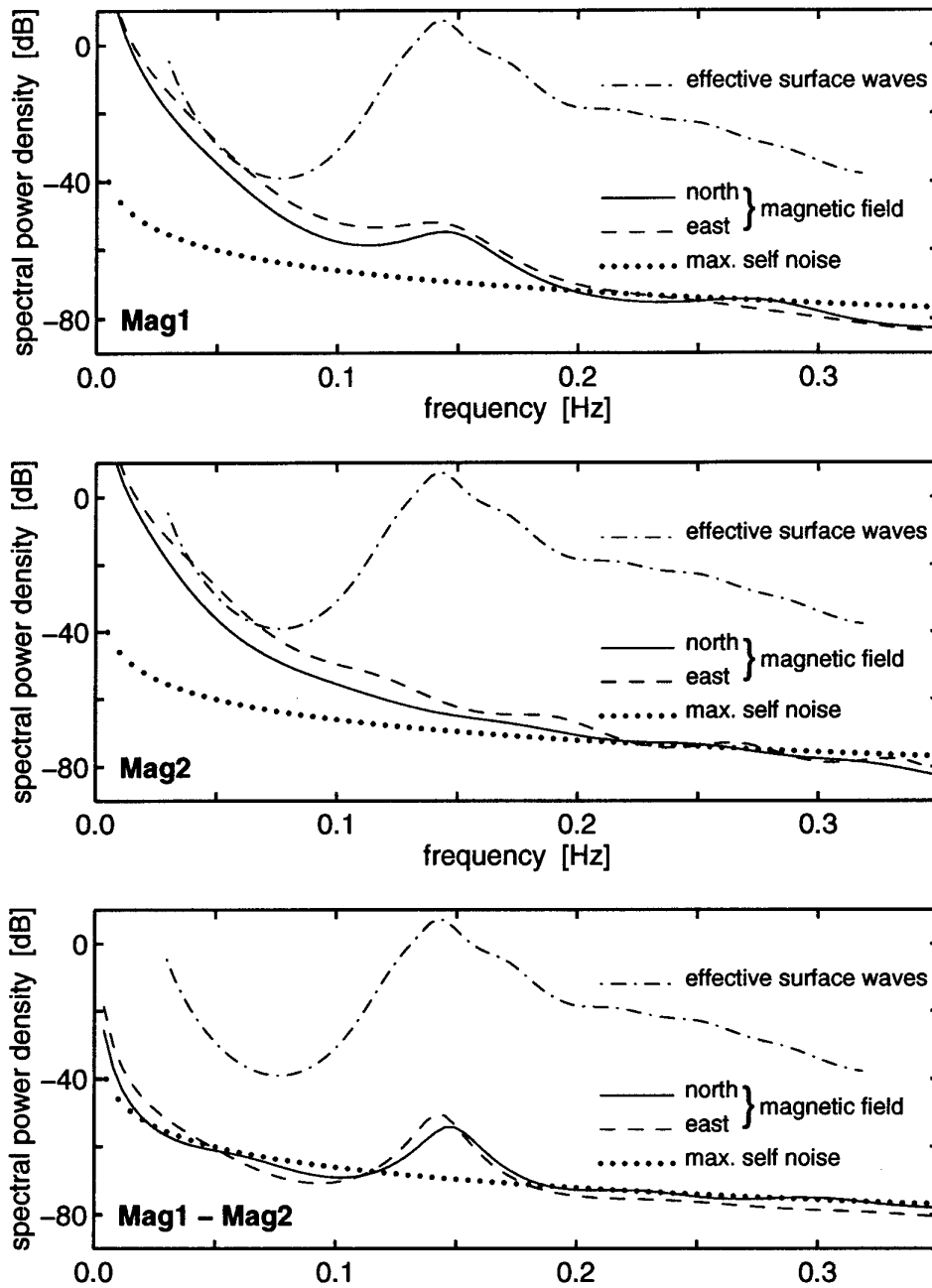
Figure 4 *ME spectra of northward (solid) and eastward (dashed) magnetic fluctuations recorded at sites M1 (top panel) and M2 (centre panel); ME spectra of magnetic field difference between sites M1 and M2 (lower panel). Effective sea surface wave spectrum (dash-dotted) and magnetometer system noise (heavily dotted) identical in all three panels. 0-dB level is equivalent to 1 nT²/Hz (magnetic field) and 1 m²/Hz (surface waves).*

Ocean waves and magnetic field differences
Formica Grande di Grosseto, 95/09/14, 01:11–04:11 UTC
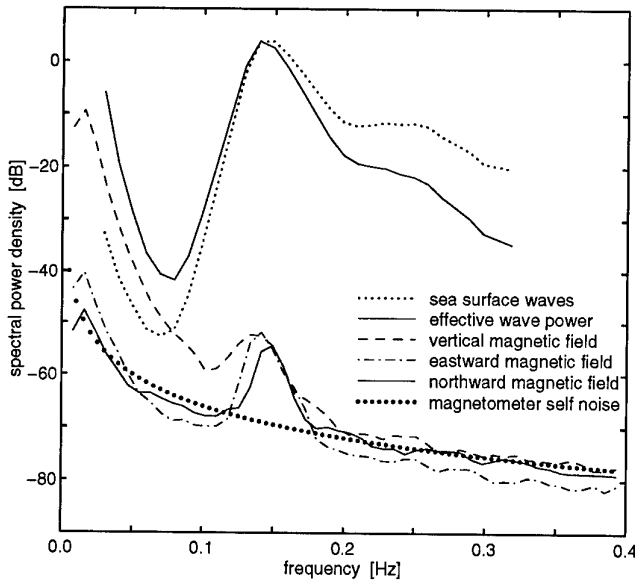
Figure 5 *Welsh periodogram estimates of northward (solid), eastward (dash-dotteded) and vertical (dotted) magnetic field differences between sites M1 and M2; uncorrected and effective corrected sea surface wave spectra for the same time interval (dotted and heavy solid lines, respectively); magnetometer system noise (heavily dotted). 0 dB is equivalent to 1 nT²/Hz (magnetic field oscillations) and 1 m²/Hz (surface waves*
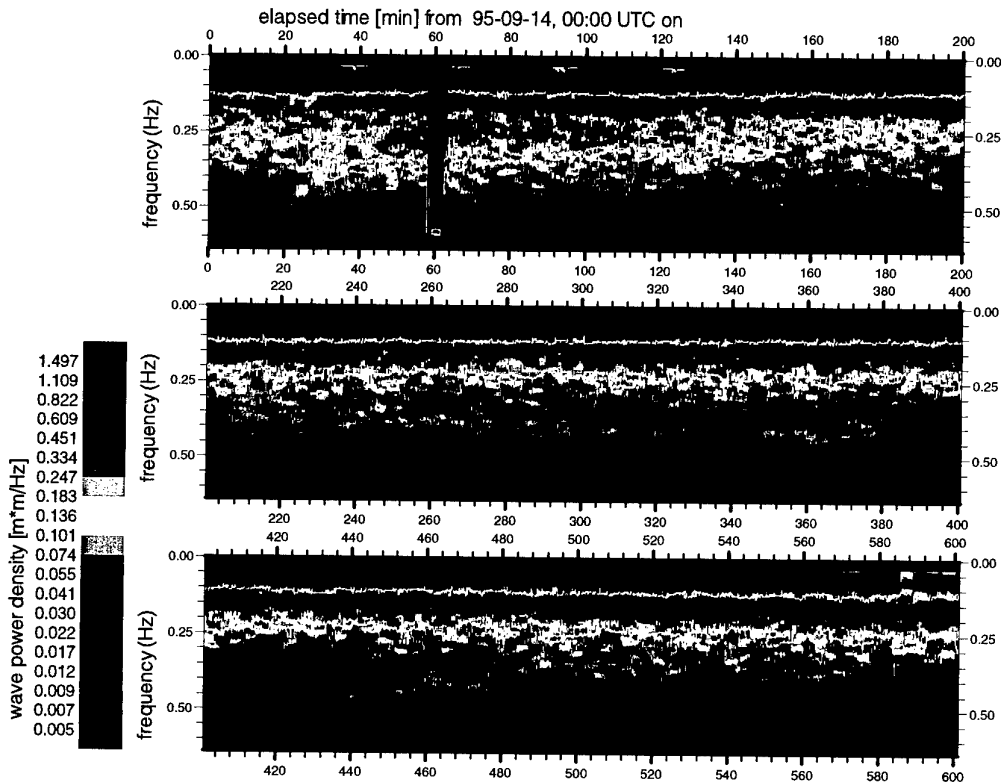
Figure 6 *Running power density spectra of swell. Time interval covered: 95/09/14, 00:00- 10:00 UTC. Time axis (annotated in elapsed minutes) starts at left edge of upper panel, runs to the right, continues at left edge of second panel, and so forth. In each panel, frequency increases from top to bottom. Color scaling bar on the left hand side.*

Spectral parameters of magnetic field difference vector

Formica Grande di Grosseto, 95/09/14, 01:11–07:11 UTC
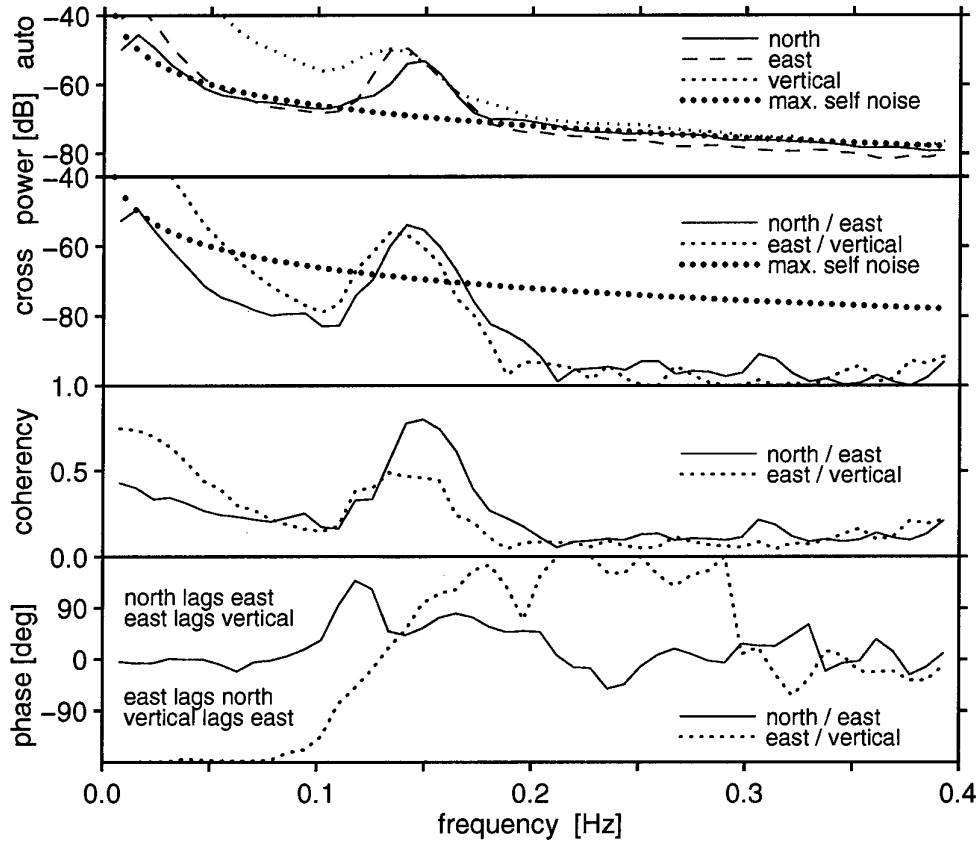

Figure 7 *Welsh periodogram estimates of northward (solid), eastward (dashed) and vertical (dotted) magnetic field differences, with maximum system self noise (heavily dotted) for comparison. Top box: auto spectra; second box: cross amplitude spectra north/east and east/vertical; third box: coherency spectra north/east and east/vertical; bottom box: cross phase spectra north/east and east/vertical. 0-dB level as in previous figures. North/east coherency in excess of 0.5 in shaded area; east/vertical coherency in excess of 0.45 in left-hand section of shaded area*

Figure 8 *Ellipse (not to scale): projection into horizontal plane of mean swell-associated water mass motion close to the southern shore of Formica Grande. Shade of gray indicates vertical displacement of water mass elements (darker=lower, lighter=higher). Polarization sense indicated by curved arrows. Long arrow: propagation direction of swell coming from the Strait of Bonifacio.*

direction from
Strait of Bonifacio
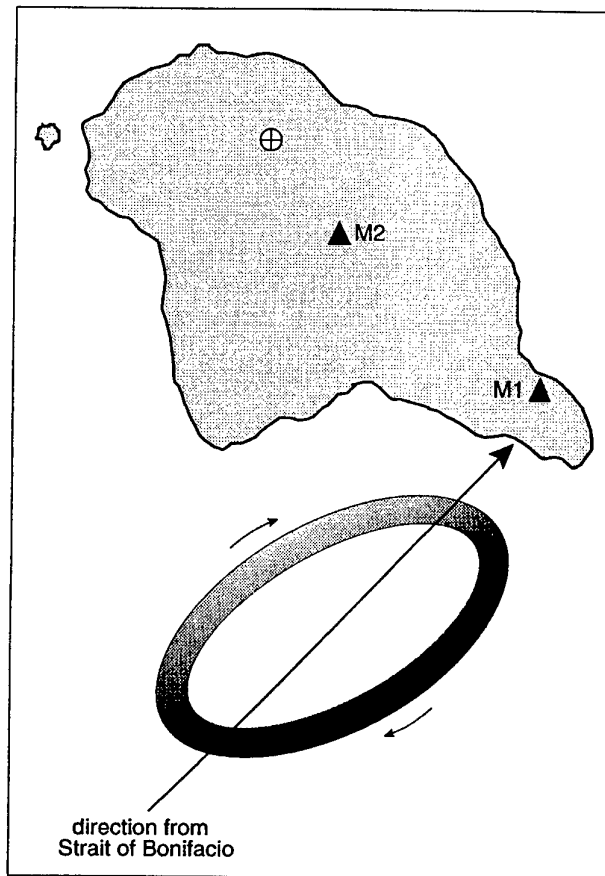
Magnetic dynamo field versus swell
### Formica Grande di Grosseto, 1995
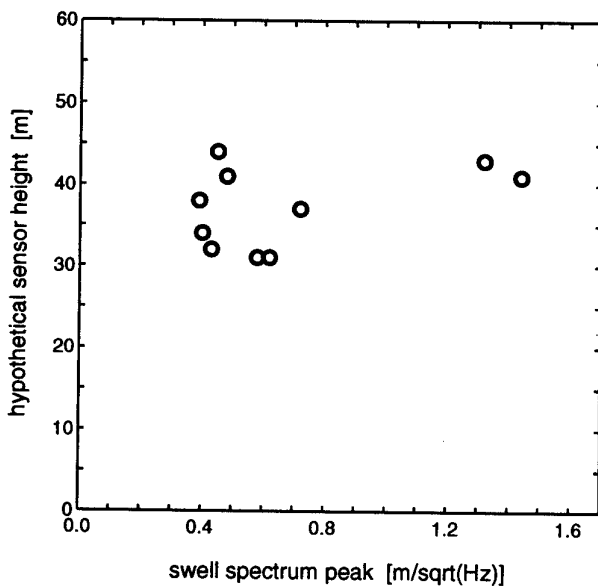
Figure 9 *Hypothetical magnetometer height plotted against the swell spectral peak amplitude. Each of the ten points represents one event representing a time series segment of three hours length. The ten events were selected from four different nights.*
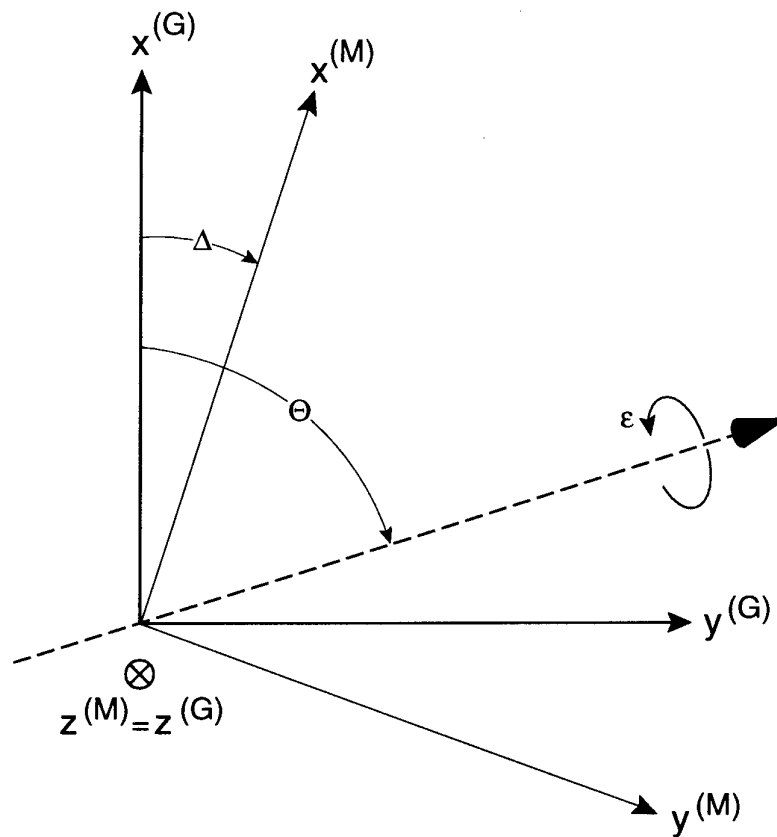
Figure A1 *Terms used in describing the magnetometer module axis system,* $x^{(M)}$ *,*
$y^{(M)}$*,* $z^{(M)}$*, with respect to the orientation of the geomagnetic reference system,* $x^{(G)}$ *,*
$y^{(G)}$*,* $z^{(G)}$*. It is assumed that the module is placed in a perfectly horizontal position*
with $z^{(M)} = z^{(G)}$ *pointing downward, out of the drawing plane.* $x^{(M)}$*,* $x^{(G)}$*,*$y^{(M)}$*,* $y^{(G)}$ *ly in*
the drawing plane, Δ *is the declination and* Θ *the bearing of the wave crest axis.* ε
denotes the (time-dependent) angle of rotation of the oscillating module.

Ocean wave and magnetic field spectra
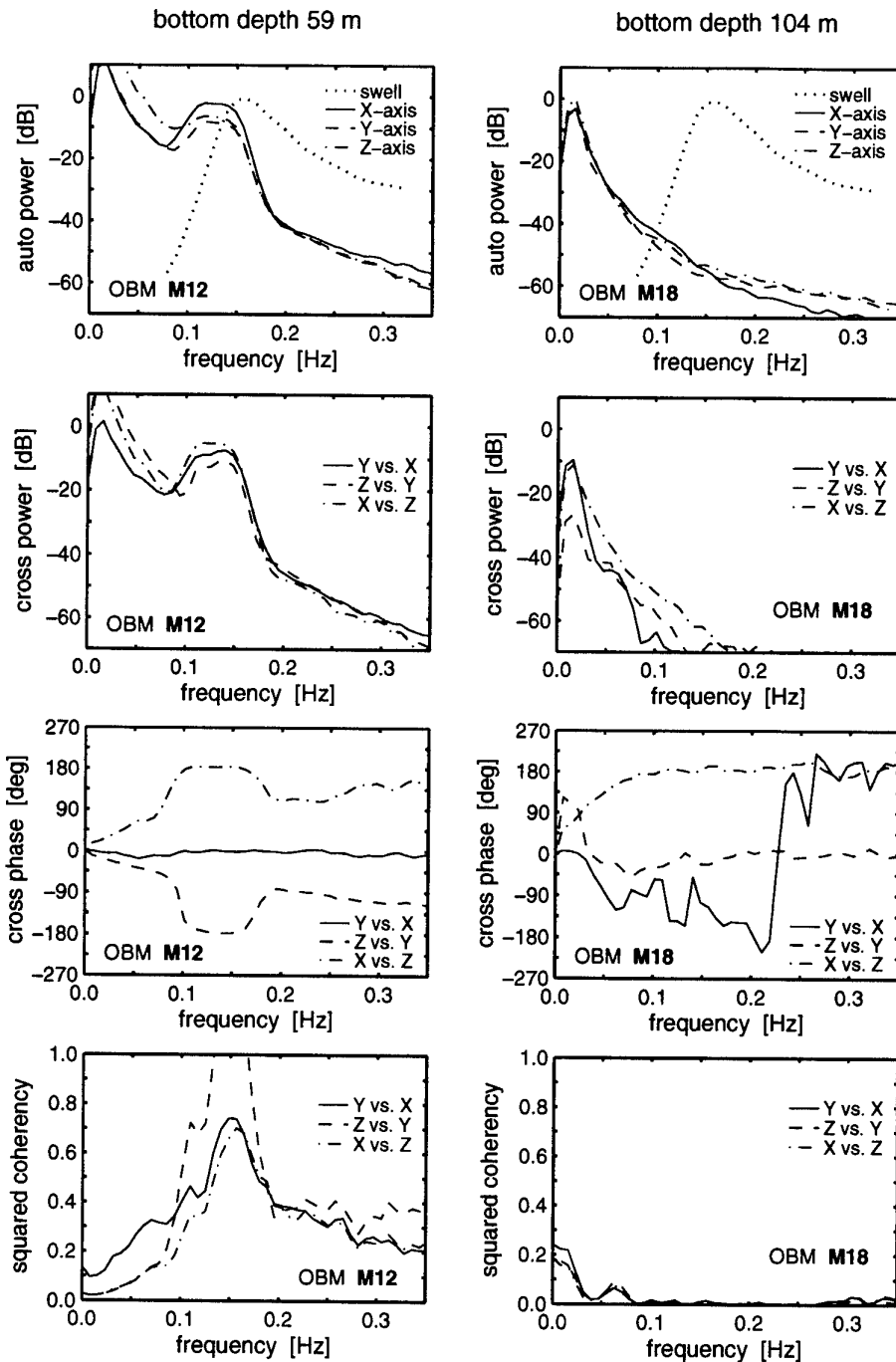
Figure A2 *Comparison of spectral parameters from wave rider measurements and from OBM recordings. Top panel: auto power spectra; second panel: cross power spectra; third panel: cross phase spectra; bottom panel: squared coherency. The latter three panels refer to measurements made along pairs of magnetometer axes. The magnetometer at 59 m depth was mechanically affected by ocean waves, the magnetometer at 104 m depth not.*

Progressing waves and magnetometer motion

OBM M12 (at 59 m depth) and wave rider (on surface)

Formica Grande di Grosseto, 95/09/15, 11:00–17:00 UTC
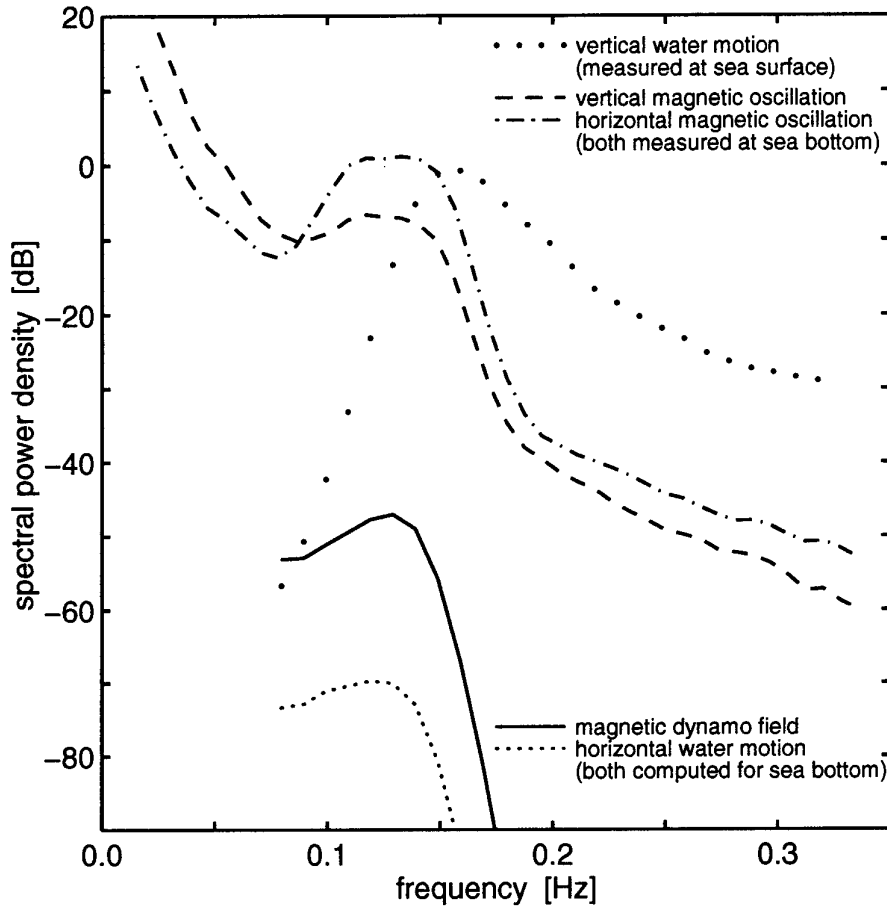
Figure A3 *Auto power density spectra of the apparent magnetic field oscillations along the ocean wave propagation vector (horizontal) and downward (vertical), recorded with OBM M12. For comparison, auto power density spectra of the wave height (equivalent to the vertical water motion at the sea surface), measured with the wave rider, and of the horizontal water motion close to the sea bottom (computed from the surface wave spectrum). Magnetic dynamo field expected at the sea bottom (also computed from the surface wave spectrum).*

Document Data Sheet

Security Classification	Project No.
UNCLASSIFIED	061-1

Document Serial No.	Date of Issue	Total Pages
SR-264	September 1997	39 pp.

Author(s)

Watermann, J.

Title

The ocean wave dynamo: a source of magnetic ambient noise

Abstract

The electromagnetic dynamo field of sea surface waves, a consequence of the Lorentz force, has been measured with two simultaneously operating, closely spaced tri-axial magnetometers. Measurements from a magnetometer located in the centre of a small, uninhabited island served to compensate measurements from a near-shore magnetometer for large-scale magnetic pulsations (basically of ionospheric origin), leaving the ocean wave dynamo field, effective close to shore only, as the dominant residual magnetic field. Height and period of waves and swell were recorded with a vertical accelerometer (wave rider buoy) floating nearby on the sea surface. Amplitude and phase relationships between the three vector components of the magnetic field differences yield an ocean wave vector consistent with swell propagating northeastward. The magnetic field data further demonstrate that the water mass motion close to shore was not confined to a vertical plane (as would be the case for freely propagating gravity waves in the open ocean). The motion occurred in a plane inclined at about 40° from the horizontal (roughly twice the inclination of the island flanks).

Ten night-time intervals of three hours each were analysed, and for every interval, the peak power of the surface waves (inferred from the wave rider measurements) was compared with the peak power of the residual horizontal magnetic field (after the background field had been removed). Their ratio yields the height of a hypopthetical magnetometer above the surface of the open sea. Not only are the hypothetical heights computed for the ten different intervals similar, they are also approximately equal to the horizontal distance between the shoreline and the site of the near-shore magnetometer.

Our results suggest that the island-based dual-sensor magnetic field observations yield, within the limits of statistical significance, a reproducible quantitative description of the amplitude and frequency of sea surface waves and swell, and of the mean water mass motion within about one wavelength from shore. Our results further suggest that the surface wave dynamo field is in quantitative agreement with predictions from classical theory. We can not confirm reports in the technical literature about an allegedly excessively intense ocean wave dynamo field.

Keywords

Initial Distribution for SR 264

Ministries of Defence		Scientific Committee of National Representatives	
DND Canada	10	SCNR Belgium	1
CHOD Denmark	8	SCNR Canada	1
DGA France	8	SCNR Denmark	1
MOD Germany	15	SCNR Germany	1
HNDGS Greece	12	SCNR Greece	1
MARISTAT Italy	9	SCNR Italy	1
MOD (Navy) Netherlands	12	SCNR Netherlands	2
NDRE Norway	10	SCNR Norway	1
MOD Portugal	5	SCNR Portugal	1
MDN Spain	2	SCNR Spain	1
TDKK and DNHO Turkey	5	SCNR Turkey	1
MOD UK	20	SCNR UK	1
ONR USA	42	SCNR USA	2
		French Delegate	1
		SECGEN Rep. SCNR	1
NATO Commands and Agencies		NAMILCOM Rep. SCNR	1
NAMILCOM	2		
SACLANT	3	**National Liaison Officers**	
CINCEASTLANT/			
COMNAVNORTHWEST	1	NLO Canada	1
CINCIBERLANT	1	NLO Denmark	1
CINCWESTLANT	1	NLO Germany	1
COMASWSTRIKFOR	1	NLO Italy	1
COMMAIREASTLANT	1	NLO Netherlands	1
COMSTRIKFLTANT	1	NLO Spain	1
COMSUBACLANT	1	NLO UK	1
SACLANTREPEUR	1	NLO USA	1
SACEUR	2		
CINCNORTHWEST	1		
CINCSOUTH	1		
COMEDCENT	1		
COMMARAIRMED	1		
COMNAVSOUTH	1	**Sub-total**	**208**
COMSTRIKFORSOUTH	1		
COMSUBMED	1	SACLANTCEN	30
NC3A	1		
PAT	1	**Total**	**238**